Semi-analytical model for electrically injected monolithic GaAs on silicon nano-ridge laser diodes

Andualem Ali Yimam, Geert Morthier and Dries Van Thourhout
Ghent University, Department of Information and Technology (INTEC), Photonics Research Group, iGent, Technologiepark-Zwijnaarde 126, 9052 Ghent, Belgium

Abstract

In the field of silicon photonics, monolithic integration of III-V materials on silicon is considered the ultimate integration approach in terms of scalability and reduced cost but it is quite challenging due to the large mismatch in crystal lattice constants, polarity and thermal expansion coefficients. Large mismatches in lattice constants and polarity lead to formation of defects severely limiting the carrier lifetime, thereby hampering efficient light emission. By employing selective area growth over confined regions to restrict defects in narrow oxide trenches, nano-ridge engineering was recently introduced to grow the III-V material out of the trench for high modal gain. Here, we present a semi-analytical model that can accurately explain the working principle behind electrically injected $In_{0.2}Ga_{0.8}As$/GaAs on silicon monolithic nano-ridge laser diodes and discuss how the model can be used to study the spectral behavior and the threshold gain. Analytical expressions for codirectional mode coupling are used in developing the round-trip laser model. Results from analytical expressions are verified by comparing them with Ansys Lumerical Finite Difference Time Domain (FDTD) simulation results.

1. Introduction

Research on monolithically integrated lasers has been ongoing in our group and imec for quite some time now. By employing the nano-ridge engineering technique [1], optically pumped $In_{0.2}Ga_{0.8}As$/GaAs multi-quantum well nano-ridge lasers emitting around 1020nm were reported [2]. Given the small dimensions of these devices, electrical pumping remains challenging but was successfully demonstrated exploiting a mode beating effect to reduce losses [3]. Continuous-wave lasing at room temperature for nano-ridge laser arrays with emission wavelength around 1020nm was achieved. In these lasers, three $In_{0.2}Ga_{0.8}As$ quantum wells (QW's) were used as gain material in a GaAs base and an InGaP passivation layer cap was used to effectively suppress surface recombination. GaAs p-i-n diodes were realized by a tungsten contact that lands on a heavily doped n-type Si surface on which the n-type GaAs trench region is grown and by another tungsten grating contact that pierces the InGaP cap and lands on the p-type GaAs. Here, we develop a semi-analytical model for these electrically injected $In_{0.2}Ga_{0.8}As$/GaAs nano-ridge lasers. The model helps not only in understanding the internal operation of these devices but also in optimizing the cross-sections of the device and metal contact grating scheme for low threshold gain and defining the emission wavelength. We will explore in this work that beating between the modes of the nano-ridge is central in the lasing operation.

2. Coupling between modes in a nano-ridge waveguide

We consider a nano-ridge waveguide with a periodic array of tungsten plugs (with contact pitch of 4.8µm) for current injection integrated on top as shown in Figure 1(a) with a cross-section as shown in Figure 1(b) and Table 1. Using the Lumerical FDTD solver [4], we calculated the loss for the TE00 mode travelling through this structure by putting a modal source at z=0 and two power monitors at z=50µm and z=100µm and considering an exponential power decay. The simulated transmission spectrum shown in Figure 1 (c) exhibits dips in the loss. Inspecting the field pattern at 1.035µm, the wavelength with the lowest loss, we notice a beating pattern with a beating length of 1.6µm as shown in Figure 1(d). Further inspection reveals that this pattern originates from mode beating between the TE00 and TEM02 modes and results in a reduced overlap with the lossy metal.

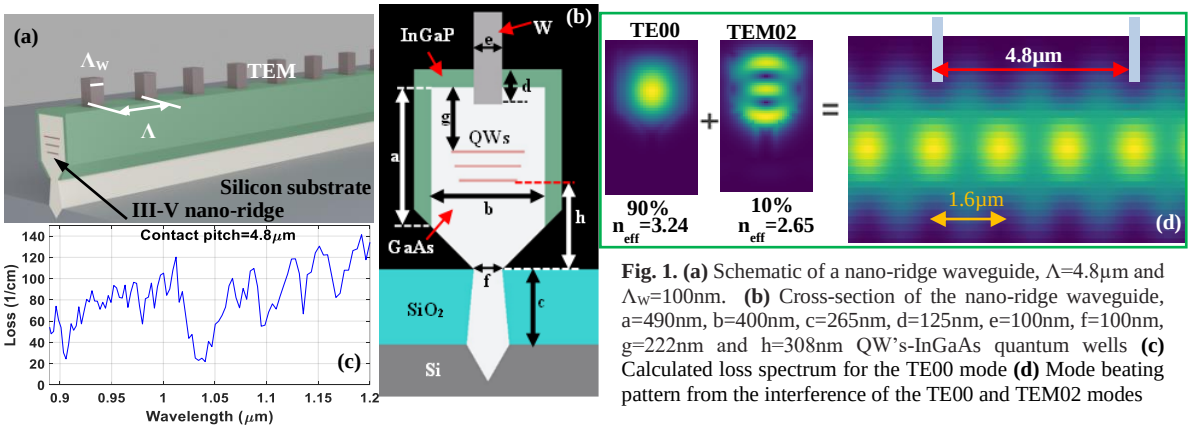

Fig. 1. (a) Schematic of a nano-ridge waveguide, Λ=4.8µm and Λ_W=100nm. **(b)** Cross-section of the nano-ridge waveguide, a=490nm, b=400nm, c=265nm, d=125nm, e=100nm, f=100nm, g=222nm and h=308nm QW's-InGaAs quantum wells **(c)** Calculated loss spectrum for the TE00 mode **(d)** Mode beating pattern from the interference of the TE00 and TEM02 modes

Table 1. Parameters for GaAs Nano-ridge Cross-section in Fig. 1 (b)

a(nm)	b(nm)	c(nm)	d(nm)	e(nm)	f(nm)	g(nm)	h(nm)
490	400	265	125	100	100	222	308

Considering two modes in the nano-ridge waveguide, the total electric field in the waveguide can be given by:

$$E(x,y,z) = E_1(z)U_1(x,y)e^{-j\beta_1 z} + E_2(z)U_2(x,y)e^{-j\beta_2 z} \quad (1)$$

where $U_1(x,y)$ and $U_2(x,y)$ are the mode profiles of the unperturbed waveguide, β_1 and β_2 are unperturbed propagation constants of the modes and E_i's are mode amplitudes.

Using the Helmholtz equation for the total electric field and assuming a perturbation with a rectangular $\Delta\varepsilon$ profile for the relative dielectric constant, we can derive the following coupled wave equations by keeping only the slowly varying terms as:

$$\frac{dE_1}{dz} = -j\kappa_{11}E_1 - j\kappa_{12}E_2 e^{j\left(\beta_1-\beta_2-l\frac{2\pi}{\Lambda}\right)z} \quad (2)$$

$$\frac{dE_2}{dz} = -j\kappa_{22}E_2 - j\kappa_{21}E_1 e^{j\left(\beta_2-\beta_1+l\frac{2\pi}{\Lambda}\right)z} \quad (3)$$

where $\kappa_{11} = \frac{{\kappa_0}^2}{2\beta_1}\frac{\int \Delta\varepsilon_0 {U_1}^2 dA}{\int {U_1}^2 dA}$, $\kappa_{22} = \frac{{\kappa_0}^2}{2\beta_2}\frac{\int \Delta\varepsilon_0 {U_2}^2 dA}{\int {U_2}^2 dA}$, $\kappa_{12} = \frac{{\kappa_0}^2}{2\beta_1}\frac{\int \Delta\varepsilon_{-l} U_1 U_2 dA}{\int {U_1}^2 dA}$, $\kappa_{21} = \frac{{\kappa_0}^2}{2\beta_2}\frac{\int \Delta\varepsilon_l U_1 U_2 dA}{\int {U_2}^2 dA}$, k_0 is the free-space propagation constant and $l\left(\frac{2\pi}{\Lambda}\right)$ are the space harmonics of the perturbation with a fundamental period Λ (as shown in Figure 1a) and l is an integer for which $\beta_1 - \beta_2 \approx l\frac{2\pi}{\Lambda}$.

κ_{11} and κ_{22} are self-coupling terms which are caused by a difference in the index profile of the modes between the perturbed and unperturbed waveguide. κ_{12} and κ_{21} determine the coupling between the modes. For a perturbation with a rectangular $\Delta\varepsilon$ profile which is complex, κ_{12}, κ_{21}, κ_{11} and κ_{22} are all complex and can be calculated as [5]:

$$\kappa_{12} = \frac{{\kappa_0}^2}{2\beta_1(\lambda)}\frac{\sin\left(\pi\frac{\Lambda W}{\Lambda}\right)}{\pi}\Delta\varepsilon(\lambda)\frac{\int_G U_1 U_2 dA}{\int {U_1}^2 dA} \qquad \kappa_{21} = \frac{{\kappa_0}^2}{2\beta_2(\lambda)}\frac{\sin\left(\pi\frac{\Lambda W}{\Lambda}\right)}{\pi}\Delta\varepsilon(\lambda)\frac{\int_G U_1 U_2 dA}{\int {U_2}^2 dA}$$

$$\kappa_{11} = \frac{{\kappa_0}^2}{2\beta_1(\lambda)}\left(\frac{\Lambda W}{\Lambda}\right)\Delta\varepsilon(\lambda)\frac{\int_G {U_1}^2 dA}{\int {U_1}^2 dA} \qquad \kappa_{22} = \frac{{\kappa_0}^2}{2\beta_2(\lambda)}\left(\frac{\Lambda W}{\Lambda}\right)\Delta\varepsilon(\lambda)\frac{\int_G {U_2}^2 dA}{\int {U_2}^2 dA}$$

where Λ and Λ_W are as shown in Figure 1 (a) and the overlap integrals (with G designation in the integrals) are evaluated over the overlap region between the fields and the metal plug.

Launching the TE00 mode at z=0, the normalized power of the modes at a position z from the source can be calculated by first solving the coupled differential equations in (1) and (2) for the electric field of the modes. The powers in the TE00 and TEM02 modes then become:

$$P_1(z) = \left(\cos(sz) - j\frac{\delta}{s}\sin(sz)\right)\left(\cos(sz) - j\frac{\delta}{s}\sin(sz)\right)^* e^{-2Im(\tilde{\beta})z} \quad \text{For the TE00 mode} \quad (4)$$

$$P_2(z) = \left(\frac{\kappa_{21}}{s}\sin(sz)\right)\left(\frac{\kappa_{21}}{s}\sin(sz)\right)^* e^{-2Im(\tilde{\beta})z} \quad \text{For the TEM02 mode} \quad (5)$$

where $\tilde{\beta} = \frac{\beta_1(\lambda)+\kappa_{11}(\lambda)+\beta_2(\lambda)+\kappa_{22}(\lambda)}{2}$ $\delta = \frac{\beta_1(\lambda)+\kappa_{11}(\lambda)-\beta_2(\lambda)-\kappa_{22}(\lambda)}{2} - l\frac{\pi}{\Lambda}$ $s(\lambda) = \sqrt{\delta^2(\lambda) + k_{12}(\lambda)k_{21}(\lambda)}$

$\beta_1(\lambda) = \frac{2\pi}{\lambda}n_{1nr}(\lambda)$ $\beta_2(\lambda) = \frac{2\pi}{\lambda}n_{2nr}(\lambda)$

All the terms $\tilde{\beta}, \delta, s, \beta_1, \beta_2$ and the coupling coefficients are wavelength dependent. The fundamental period for this instance is $\Lambda = 4.8\mu m$ and $n_{1nr}(\lambda)$ and $n_{2nr}(\lambda)$ are the unperturbed effective indices of the two modes in the nano-ridge. Exporting electric field data, effective refractive indices for the two modes and permittivity data from FDE Mode and calculating overlap integrals by performing numerical integration in Matlab, we evaluated the coupling coefficients and calculated the power spectrum of the two modes at different positions from the source and compared these results with FDTD simulation results. Figure 2 (a) shows a comparison between analytical results and simulation results for the power in the TE00 and TEM02 modes in the 890-1200nm wavelength range at different positions along the length of the nano-ridge and Figure 2 (b) shows the comparison for the maximum power of the modes (at the wavelength of zero detuning) at different positions along the nano-ridge length.

We can observe from these graphs that around the 1.035μm wavelength, where the coupling between TE00 and TEM02 mode coupling occurs, the results from the analytical expressions and the simulations are in agreement. In addition, Figure 2 (b) shows that in the first 60μm length span, there is a rapid decline in the power of the TE00 mode and a progressive increase in the TEM02 mode power. Beyond this position, the interference created between the two modes creates low intensity zones below the metal plugs that effectively decrease not

only the loss due to metal absorption but also the coupling between the modes. Hence, a sort of quasi-zero loss equilibrium condition is reached beyond this position where the power in the two modes decreases gently and they propagate in tandem sustaining the beating pattern.

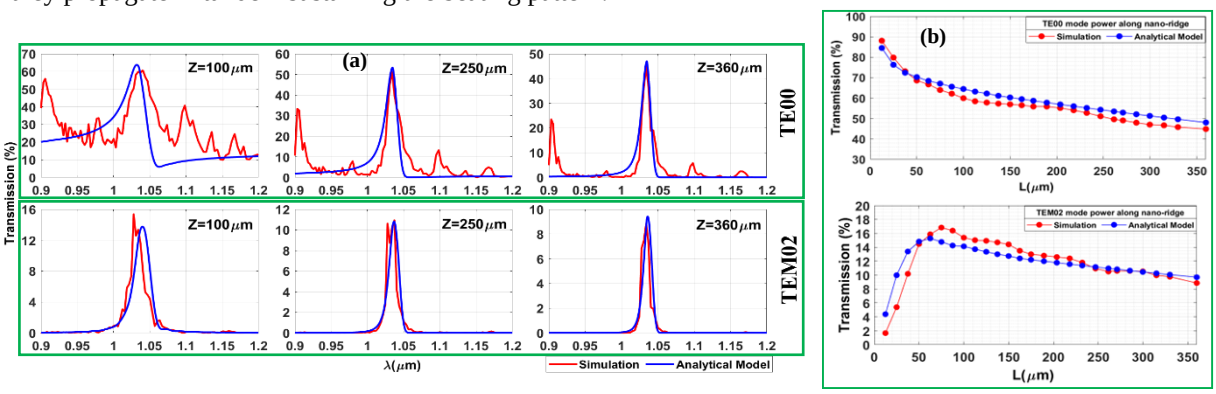

Fig. 2. Comparison between analytical results and simulation results of: **(a)** TE00 and TEM02 mode power spectra at different positions along the length of nano-ridge waveguide. **(b)** TE00 and TEM02 mode power at zero detuning wavelength at different z positions from the source.

3. Round-trip Laser Model

To develop a model for the round-trip gain, we start from the left facet and consider the general case where TE00 and TEM02 modes are launched with normalized amplitudes of a_1 and a_2. The modes propagate a length L and reach the right facet with normalized amplitudes of $a_1{}'$ and $a_2{}'$. Upon reflection, we have $b_1{}'$ and $b_2{}'$ which again propagate a length L and reach the left facet and get reflected from this facet with normalized amplitudes of b_1 and b_2. Utilizing results of codirectional coupling between the TE00 and TEM02 modes, discussed in the previous section, we have for a round-trip

$$\begin{bmatrix} b_1 \\ b_2 \end{bmatrix} = \begin{bmatrix} r_{11} & r_{12} \\ r_{21} & r_{22} \end{bmatrix} \begin{bmatrix} (cos(sL) - j\frac{\delta}{s}\sin(sL))e^{-j\left(\tilde{\beta}+l\frac{\pi}{\Lambda}\right)L} & -j\frac{\kappa_{12}}{s}\sin(sL)\, e^{-j\left(\tilde{\beta}+l\frac{\pi}{\Lambda}\right)L} \\ -j\frac{\kappa_{21}}{s}\sin(sL)\, e^{-j\left(\tilde{\beta}-l\frac{\pi}{\Lambda}\right)L} & (cos(sL) + j\frac{\delta}{s}\sin(sL))e^{-j\left(\tilde{\beta}-l\frac{\pi}{\Lambda}\right)L} \end{bmatrix}$$
$$\times \begin{bmatrix} r_{11} & r_{12} \\ r_{21} & r_{22} \end{bmatrix} \begin{bmatrix} (cos(sL) - j\frac{\delta}{s}sin(sL))e^{-j\left(\tilde{\beta}+l\frac{\pi}{\Lambda}\right)L} & -j\frac{\kappa_{12}}{s}sin(sL)e^{-j\left(\tilde{\beta}+l\frac{\pi}{\Lambda}\right)L} \\ -j\frac{\kappa_{21}}{s}sin(sL)e^{-j\left(\tilde{\beta}-l\frac{\pi}{\Lambda}\right)L} & (cos(sL) + j\frac{\delta}{s}sin(sL))e^{-j\left(\tilde{\beta}-l\frac{\pi}{\Lambda}\right)L} \end{bmatrix} \begin{bmatrix} a_1 \\ a_2 \end{bmatrix} \quad (6)$$

where reflection scattering coefficients at the facets are defined as: $r_{11} = \frac{b_1{}'}{a_1{}'}|\ a_2{}' = 0, r_{12} = \frac{b_1{}'}{a_2{}'}|\ a_1{}' = 0,\ r_{21} = \frac{b_2{}'}{a_1{}'}|\ a_2{}' = 0$ and $r_{22} = \frac{b_2{}'}{a_2{}'}|\ a_1{}' = 0$. We evaluated these reflection coefficients by FDTD simulations from one cleaved facet to be $r_{11} = 0.60$, $r_{12} = r_{21} = 0.24$ and $r_{22} = 0.82$. The other parameters are as defined in section 2, except that the propagation constants now also include gain and extra losses. The losses are due to scattering, leakage to substrate and free-carrier absorption in doped regions i.e. $\beta_1 = \frac{2\pi}{\lambda}n_{1nr} + j\frac{1}{2}\Gamma_{xy1}g_m - j\frac{1}{2}\alpha_{dop1} - j\frac{1}{2}\alpha_{scat1}$, $\beta_2 = \frac{2\pi}{\lambda}n_{2nr} + j\frac{1}{2}\Gamma_{xy2}g_m - j\frac{1}{2}\alpha_{dop2} - j\frac{1}{2}\alpha_{scat2}$, $\Gamma_{xy1} = \frac{\int_{QW}{U_1}^2 dA}{\int {U_1}^2 dA}$ and $\Gamma_{xy2} = \frac{\int_{QW}{U_2}^2 dA}{\int {U_2}^2 dA}$. Γ_{xy1} and Γ_{xy2} are the transverse confinement factors for the TE00 and TEM02 modes in the three $In_{0.2}Ga_{0.8}As$ quantum well (QW) regions respectively hence the designation QW in the overlap integrals. g_m is the material gain for the quantum wells. α_{dop1} and α_{dop2} correspond to losses associated with free-carrier absorption in doped regions and α_{scat1} and α_{scat2} are nano-ridge waveguide losses due to scattering and leakage to substrate for TE00 and TEM02 modes respectively. The scattering and leakage to substrate losses were measured on fabricated undoped nano-ridge waveguides using a Fabry-Perot interferometric method [6]. A loss arising from scattering and leakage to substrate of 8 $\pm$0.5/cm was then calculated for a 3.5mm long device. Similar results were obtained for varying waveguide sizes and device lengths. Furthermore, the free-carrier absorption losses in doped regions for TE00 and TEM02 modes were calculated with the Lumerical FDE Mode solver by introducing the imaginary part of the refractive indices of doped materials in the solver. Consequently, the loss due to free-carrier absorption in doped regions is 5.2/cm and 11.6/cm for TE00 mode and TEM02 mode respectively.

Lasing will occur for an eigenvalue 1 of the 2x2 matrix (product of the first four matrices on the right side of (6)). We calculated the threshold gain to be 792/cm for a device length of 1502.4μm by a self-written Matlab code where we developed an iterative process that starts with a certain gain value and solves for the eigenvalue magnitude till we obtain an eigenvalue magnitude of 1 by making small changes in the gain. Figures 3 (a) and 3 (b) show the calculated eigenvalue magnitude and phase. Points in red color are wavelength points with zero phase and the point at 1035.65nm satisfies the laser condition as shown in Figure 3 (b) and (c). Meanwhile, the

eigenvector corresponding to this matrix with an eigenvalue of 1 gives a certain combination of a_1 and a_2 that leads to lasing in the cavity. We can see from Figure 3 (d) that 89% of TE00 and 11% of TEM02 is the combination of modes that case lase around 1.035µm.

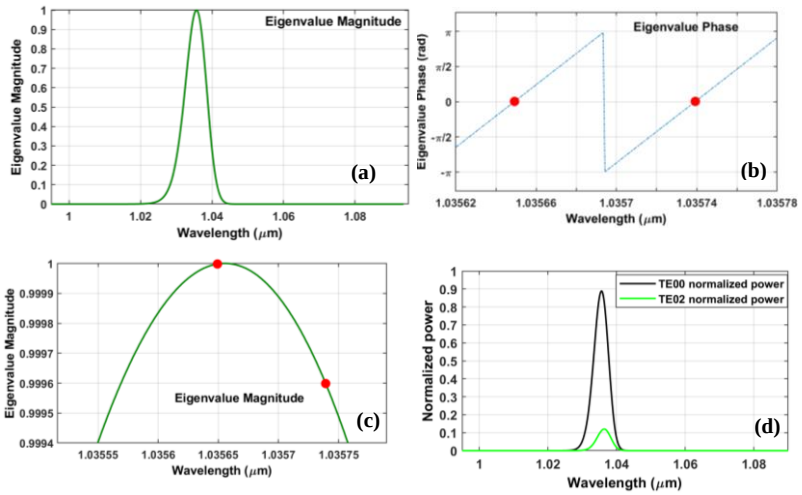

Fig. 3. (a) Eigenvalue magnitude **(b)** Eigenvalue phase (points in red color have zero phase and a magnitude close to 1) **(c)** Eigenvalue magnitude around zero detuning wavelength (points in red color have eigenvalue phase of zero) **(d)** Eigenvector (combination of TE00 and TEM02 modes that lead to a lasing condition).

4. Conclusion

In conclusion, we presented a semi-analytical model that saves lots of computational resources and simulation time with better accuracy for electrically injected monolithic nano-ridge lasers emitting around 1035nm. We derived analytical expressions that explain the codirectional coupling between modes in a nano-ridge waveguide with a tungsten metal contact grating on top and verified the results by using the 3D Lumerical FDTD solver. The interference created between the fundamental TE00 mode and a higher order mode results in low intensity zones below the metal plugs that effectively decrease not only the loss due to metal absorption but also the coupling between the modes, leading to a sort of quasi-zero loss equilibrium condition where the power in the two modes decreases gently. This has allowed loss dips that enabled laser operation. By extracting mode effective refractive indices, electric field data, reflection scattering coefficients, free-carrier absorption losses due to dopants and mode confinement factors from Lumerical FDTD and FDE simulations, we showed how the round-trip model helps in investigating the spectral behavior and the threshold gain.

5. Acknowledgement

This work was supported by the EU H2020 under grant agreement No. 884963 (ERC AdG NARIOS).

References

1. B. Kunert et al., "Integration of III/V Hetero-structures by Selective Area Growth on Si for Nano- and Optoelectronics," ECS Trans. 75(8), 409–419 (2016).
2. Y. Shi et al., "Optical pumped InGaAs/GaAs nano-ridge laser epitaxially grown on a standard 300-mm Si wafer," Optica 4(12), 1468 (2017).
3. Y. De Koninck et al., "GaAs nano-ridge laser diodes fully fabricated in a 300mm CMOS pilot line," arXiv:2309.04473, (Sept. 2023).
4. Ansys Lumerical photonics simulation and design software official website, URL https://www.ansys.com/products/photonics
5. K. David et al., "Coupling coefficients in gain-coupled DFB lasers: Inherent compromise between coupling strength and loss," IEEE Photonics Technol. Lett. 3(5), 439–441 (1991).
6. Sareh Taebi et al., "Modified Fabry–Perot interferometric method for waveguide loss measurement", Optical Society of America, Applied Optics, Vol. 47, No. 35 (2008).

21. A computationally efficient tool for calculating the field in a multi-mode fiber
Bernat Molero Agudo

22. Dissipative coupling between ring resonators for large area, single mode lasing at visible wavelengths
Korneel Molkens

23. Micro-Transfer Printing for cm-scale Heterogeneous Integration of Lithium Niobate
Margot Niels

24. Influence of waveguide taper length on the total loss of an Al2O3:Er3+ – Si3N4 vertical coupler
Carlos Osornio Martinez

25. Comparison of annealing methods for photonic Ising machines
Toon Sevenants

26. Fluctuation imaging of nanoscale disorder in monolayer semiconductors
Tom Sistermans

27. Design and Fabrication of Low Loss SiOx Waveguide for Applications in the UVC wavelength range
Chenming Su

28. Low-loss Hybrid Optical Waveguides in Amorphous Silicon Carbide
Mohammad Talebi Khoshmehr

29. Complex vector fitting toolbox: a Python package for the baseband macromodeling of multi-wavelength linear and passive photonic integrated circuits
Thijs Ullrick

30. Modeling of programmable lenses with liquid crystal elastomers
Vincent van der Doef

31. Printable Optical Nonlinearities: Micro-Transfer Printing of Periodically-Poled Lithium Niobate
Tom Vandekerckhove

32. A Non-Invasive Pre-Bonding Screening Method for Cascaded SOA-based Photonic Integrated Circuits
Xudong Wang

33. Design of Subwavelength-thick metalenses with polarization-insensitive
Yunjie Yan

34. Semi-analytical model for electrically injected monolithic GaAs on silicon nano-ridge laser diodes
Andualem Yimam

35. Investigating factors influencing the reflectivity of aluminum thin layers on 3D printed micromirrors
Yaxiang Zeng

36. Integrated Gyroscope Performance for Wide Temperature Range using SiN Ring Resonators
Limeng Zhang

37. UV photonics integrated circuit for biomolecule detection with SiO2 as a waveguide core on CaF2 substrate
Xiujun Zheng

38. Directly modulated DFB lasers on InP membrane on Si
Aleksandr Zozulia

39. Aluminium oxide 1×8 splitter tree for blue light
Bjorn Jongebloed

40. On-chip Distributed Fiber Sensing based on Stimulated Brillouin Scattering
Zhizhi Yang

41. Coherent Ising machines on photonic integrated circuits
Ruqi Shi

42. Enhancing modulation efficiency and reducing transmission penalty in double-layer graphene modulators through waveguide design optimization
Tom Reep